Fabrication of Stretchable and Conductive Liquid Metal Microfibers Through Coaxial Emulsion Electrospinning

*Zihan Liu, Jiexian Ma, and Pu Zhang**

Z. Liu, J. Ma, P. Zhang
Department of Mechanical Engineering, State University of New York at Binghamton, Binghamton, NY 13902, United States
E-mail: pzhang@binghamton.edu

Keywords: liquid metal; microfiber; electrospinning; yarn

Liquid metal fibers are increasingly used in soft multifunctional materials and soft electronics due to their superb stretchability, high conductivity, and lightweight. This work presents a systematic study on the electrospinning process of liquid metal microfibers. Compared to other methods that usually produce fibers thicker than 100 microns, electrospinning is a facile and low-cost method producing liquid metal fibers in the range of 10-100 microns. Specifically, core-sheath liquid metal microfibers are fabricated with a highly-conductive liquid metal core and a super-stretchable thermoplastic elastomer sheath. This manufacturing process uses a liquid metal emulsion as the core solution, which circumvents manufacturing failures caused by the high surface tension of liquid metals. The influence of key processing parameters such as core flow rate, sheath flow rate, and applied voltage on the fiber diameter and morphology was studied by experiments. The mechanical and electrical properties of the as-fabricated liquid metal microfibers, mats, and yarns are tested and discussed.

1. Introduction

Liquid metals (LM) have become promising material candidates used in soft multifunctional materials and soft electronics. [1–7] Compared to hard conductive fillers such as silver nanowires and carbon nanotubes, LMs exhibit advantages due to their softness and fluidity, metallic feature, and high electrical conductivity. In the past decade, many different forms of LM materials have been developed and reported, e.g., LM particle composites,[8,9] short fiber composites,[10] long fiber composites,[11] lattices,[12,13] foams,[14,15] kirigami,[16] fibers,[17–19] mats,[20,21] etc. Among these materials, LM fibers offer multiple advantages and

opportunities for novel multifunctional applications.[19,22] For example, LM fibers are ideal candidates for wearable electronics, e-textiles, and fiber-based sensors due to their inherent stretchability and conductivity.[19,22,23] In addition, LM fibers can also be embedded in elastomers to produce soft conductive composites with simultaneously lightweight and high conductivity.[11]

Fabrication of LM fibers is not easy due to the high surface tension of LMs (10x of water). Various methods have been reported to fabricate LM fibers with diameters above 100 μm. We summarize these existing methods into seven categories. (i) Injecting. An early study reported an indirect way producing LM fibers by injecting LM into a hollow fiber directly.[18] The limitation is that infilling LM into thin channels face great difficulties due to the capillary effect. (ii) Drawing. One method employs the thermal drawing process of a plastic preform with a LM core.[24] The authors presented very interesting applications of these LM fibers in triboelectric energy harvesting and e-textiles. An alternative method [25,26] produces LM fibers by first injecting LM into hollow fibers and then room temperature drawing through plastic deformation. Interesting applications in wearable electronics and color-changing fibers were presented. (iii) Extrusion. This method is based on a coaxial 3D printing process.[27] The highly viscous sheath polymer melt offers the shear stress required to overcome the high surface tension on the LM core. A coaxial LM fiber can be produced by tuning the processing parameters. The production speed is slow due to the nature of the process. (iv) Direct writing. This is also a 3D printing method by direct writing of LM emulsion to overcome the surface tension obstacle.[28,29] This process also suffers from low efficiency similar to extrusion. (v) Electrochemistry. This method was primarily proposed by Dickey.[30] The surface tension of LM can be tuned by controlling the surface oxidation reactions. Continuous LM fibers as thin as 100 μm can be fabricated. A following study successfully encapsulated such LM fibers into polymers using a novel interfacial polymerization process.[31] (vi) Wet spinning. These LM fibers exhibit a core-sheath structure with a LM core and a polymer sheath.[32] The LM core can be either pure LM[32,33] or LM emulsion[17]. (vii) Coating. This method usually adds a LM coating on polymer fibers produced by direct writing[34] or electrospinning[35,36]. In brief summary, researchers have been very successful in producing LM fibers thicker than 100 μm following these mechanical, physical, or chemical methods.

There are at least three existing methods producing LM fibers thinner than 100 microns. (i) LM coating. This is achieved by simply coating a thin layer of LM on electrospun polymer fibers.[20,21] This method is very easy to implement but it also suffers from disadvantages of

smearing, relatively low conductivity, and reliability issues. (ii) Direct writing. By using a glass capillary nozzle, researchers can print thin LM lines with thickness below 10 μm.[37,38] This method achieved very high resolution, certainly with a tradeoff of the fabrication speed. (iii) Emulsion electrospinning. This method was recently developed by the authors.[11] This method used a LM emulsion as the core fluid to overcome the surface tension issue and a thermoplastic elastomer solution as the sheath fluid to maintain the mechanical strength. This method is a one-step method that encapsulates LM in the fiber directly in a facile and efficient manner. The produced fibers exhibit diameters around 10-20 microns and can be used in soft conductive composites. Among all the aforementioned methods, the emulsion electrospinning method is the most efficient one as it is driven by the electrical field. Other mechanical processes (injecting, drawing, extrusion, direct writing, and coating) or chemical processes (electrochemistry and wet spinning) are usually much slower in producing fibers. One can select the processes according to their materials and fiber diameter needs.

Overall, the emulsion electrospinning process of LM fibers is still poorly understood as it is a new process.[11] Indeed, the electrospinning of LM emulsion is quite different from polymer solutions due to the high conductivity and dielectric constant of the LM emulsion.[39,40] In order to fill this knowledge gap, this work performed a systematic study on the electrospinning process of coaxial LM fibers. The influences of core flow rate, sheath flow rate, and applied voltage on the produced fiber diameters and morphology are studied by experiments. The mechanisms underlying the electrospinning process of a highly conductive emulsion are uncovered and discussed. In addition, we also show the potential of applying the produced LM fibers as yarns for soft electronics applications, beyond the applications as conductive composites.[11]

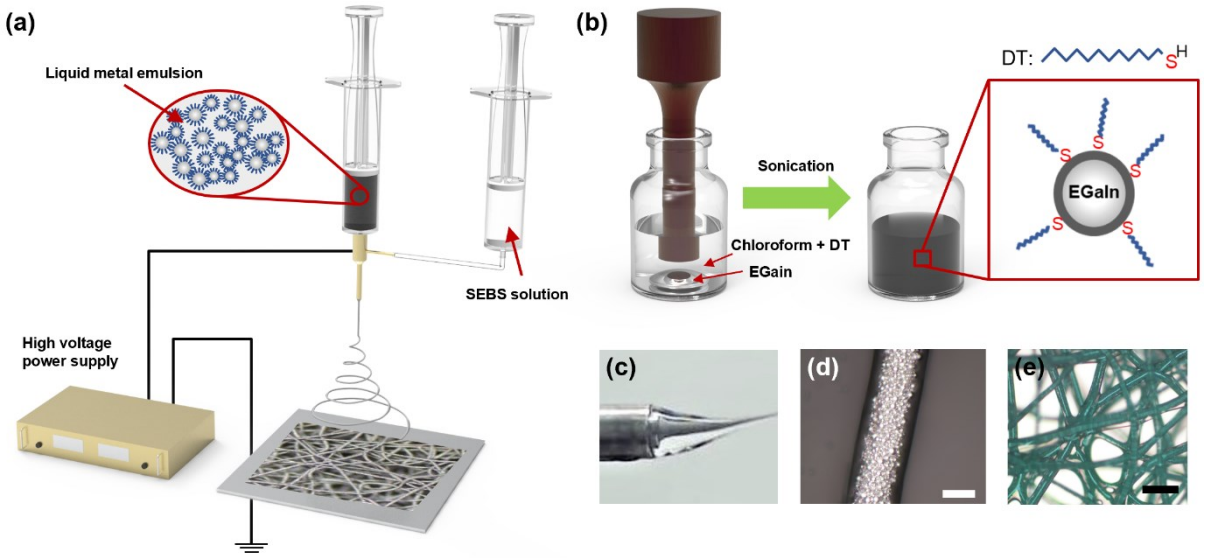

Figure 1. Coaxial emulsion electrospinning of liquid metal (LM) microfibers: (a) Schematic setup for coaxial electrospinning; (b) Synthesis of LM microparticles; (c) Compound Taylor cone; (d) Optical microscopy image of a typical coaxial LM microfiber, scale bar: 20 μm; (e) Optical microscopy image of LM fiber mat, scale bar: 200 μm.

2. Results and Discussions

2.1. Processing Study

The manufacturing process is illustrated in **Figure 1**. The coaxial emulsion electrospinning process uses LM emulsion as the core fluid and a polymer solution as the sheath fluid for encapsulation purpose. The LM particles were produced by ultrasonication. The Taylor cone and produced fibers are presented in Figure 1 as well. The recipes of the sheath solution and core emulsion are explained in what follows. We chose a thermoplastic elastomer styrene-ethylene-butylene-styrene (SEBS) as the sheath material mainly because of its high stretchability, good mechanical strength, and ease of processing. Another consideration is the fiber diameter as we seek microfibers not nanofibers. Among electrospun block copolymer fibers reported in the literature,[41] the diameters of SEBS fibers (4-12 μm) are generally much thicker than other polymers (mostly < 2 μm), although the diameters may depend on their solution concentrations. The electrospinning of SEBS fibers was well reported in the literature.[41–43] We chose a binary solvent chloroform/toluene for the sheath solution in this work. In order to optimize the SEBS concentration in the sheath solution, we first conducted electrospinning tests for pure SEBS fibers using solutions with various concentrations (10-20 wt% of SEBS). As the solution concentration increases, the SEBS fiber morphologies (Figure S1, Supporting Information) gradually changed from beads to fibers. The optimal solution

concentration was 16 wt% of SEBS in the binary solvent to produce fibers with desired diameters and smooth morphologies. Therefore, the sheath solution concentration is fixed at 16 wt% of SEBS for the coaxial emulsion electrospinning. As regard to the core emulsion, it consists of thiol coated LM particles, SEBS, and chloroform. There are two major considerations for this composition. Firstly, the emulsion should be viscous enough so that the LM particles do not sediment, which is why we added a small amount of SEBS (see the concentration in the Experimental Section). Secondly, the volume ratio between LM and SEBS should be large enough (LM:SEBS = 4:1 by volume here), otherwise the conductivity of the LM fibers will be impaired due to barriers in the percolation network and mechanical resistance against sintering. The LM particle size would affect the morphology and quality of coaxial fibers. Large particles may be easy to sinter but would induce discontinuity of the LM cores; whereas small particles usually produce uniform LM cores but are hard to sinter. Therefore, we used LM particles of 1-3 μm for the core emulsion. The particle sizes can be tuned by the ultrasonication[44] parameters (Figure S2, Supporting Information).

For coaxial emulsion electrospinning,[40,45] major processing parameters include core flow rate, sheath flow rate, voltage, and tip-to-collector distance. In fact, the electric field strength, i.e., the ratio between voltage and tip-to-collector distance, is the dominant factor influencing the electrospinning process. Hence, we fix the tip-to-collector distance as 16 cm in all experiments and only change the applied voltage. The influences of core flow rate, sheath flow rate, and voltage on the electrospinning process and fiber morphologies will be studied and introduced below.

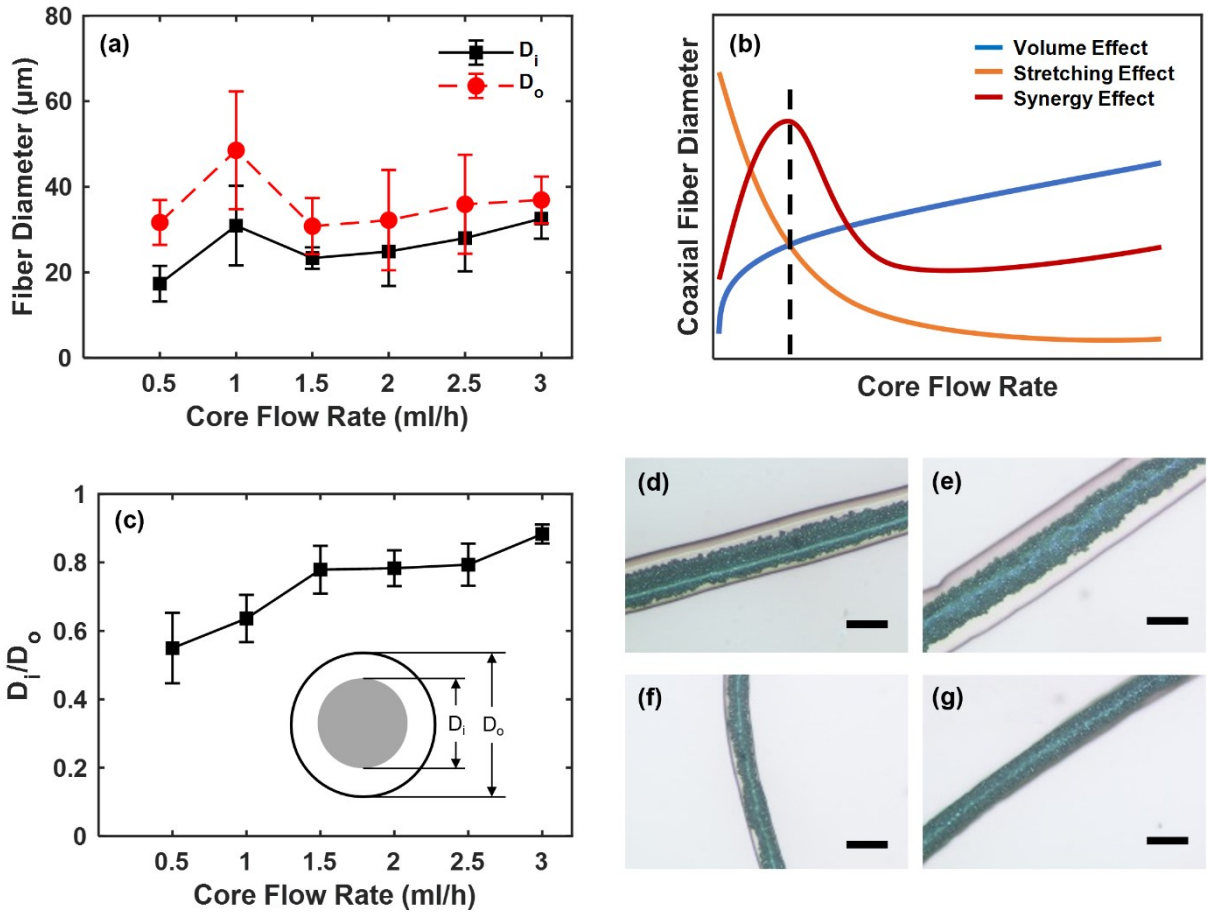

Figure 2. Effect of core flow rate on the electrospinning of coaxial LM microfibers. (a) The inner and outer diameters; (b) Competition between two mechanisms influencing fiber diameters; The synergy effect combines the volume effect and stretching effect. (c) The inner/outer diameter ratio D_i/D_o. The optical microscopy image of LM microfibers fabricated at various core flow rate as (d) 0.5 ml/h; (e) 1.0 ml/h; (f) 2.0 ml/h; (g) 3.0 ml/h, scale bar: 50 μm.

Firstly, the effect of core flow rate is studied. In this case, the sheath flow rate and applied voltage were fixed as 3.5 ml/h and 10 kV, respectively. Meanwhile, the core flow rate varied from 0.5 ml/h to 3 ml/h. Note that for electrospinning of pure polymer fibers, increasing the flow rate would usually lead to either constant[46] or increased fiber diameters[47]. In contrast, electrospinning of LM emulsion shows distinct relations. **Figure 2**a shows the influence of core flow rate on the fiber diameters of coaxial LM fibers. Both the inner diameter D_i and outer diameter D_o are presented. It was found that with the increase of core flow rate, the fiber diameters first increase and then decrease, and reach a peak when the core flow rate is 1 ml/h. This mysterious phenomenon is explained in Figure 2b. There are two competing factors

influencing the fiber diameters as the core flow rate increases. The first factor is called volume effect, because increasing the core flow rate will supply more fluid to the core-sheath fibers and lead to thicker fiber diameters, which was observed for pure polymer fibers.[47] The second factor is called stretching effect. Considering the high conductivity and dielectric constant of the LM core emulsion, higher core flow rate results in greater Coulomb force stretching the fibers and consequently thinner fiber diameters. This stretching effect was observed for electrospinning of polymer solutions with higher conductivity.[48] For LM emulsions, the volume effect and stretching effect compete with each other, resulting in the synergy effect illustrated in Figure 2b. We also compared the inner/outer diameter ratio D_i/D_o in Figure 2c, which follows a monotonically increasing trend as the core flow rate increases. This is easy to understand considering the conservation of mass. Typical fiber morphology of the microfiber samples is shown in Figure 2d-g to illustrate the influence of core flow rate on the inner/outer diameter ratios. At high core flow rates, such as 3 ml/h, the sheath layer becomes indistinguishable.

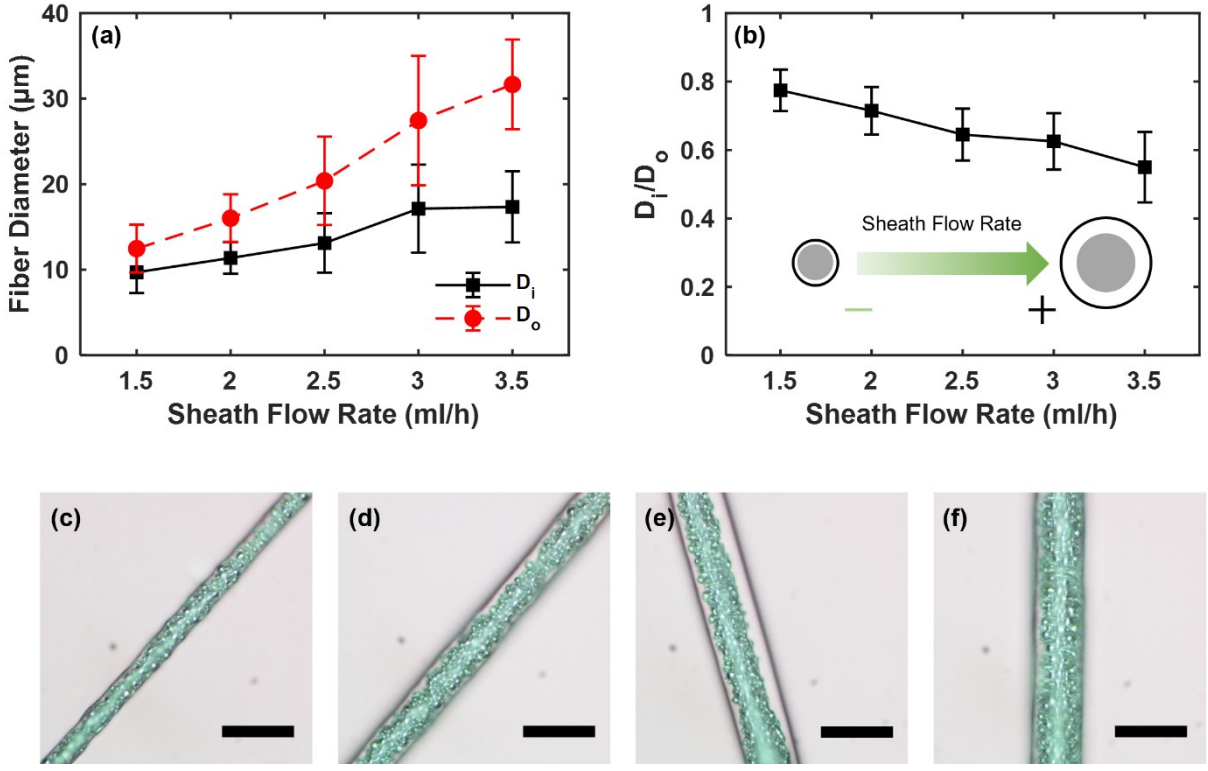

Figure 3. Effect of sheath flow rate on the electrospinning of coaxial LM microfibers. (a) The inner and outer diameters; (b) The inner/outer diameter ratio D_i/D_o. Some typical OM images of electrospun microfiber samples with different sheath flow rates: (c) 1.5 ml/h; (d) 2.0 ml/h; (e) 2.5 ml/h; (f) 3.0 ml/h, scale bar: 40 μm.

Next, the effect of sheath flow rate is studied. In this case, the core flow rate is set as 0.5 ml/h and the applied voltage is 10 kV. The sheath flow rate ranges from 1.5 ml/h to 3.5 ml/h. **Figure 3**a shows the influence of sheath flow rate to the fiber diameters. We observed that both the inner and outer diameters increase monotonically when the sheath flow rate increases. The reason is that higher sheath flow rate will thicken the sheath layer and reduce the stretching effect exerted from the electrical field. As a result, both the inner and outer diameters are larger due to less stretching. In addition, as shown in Figure 3b, the inner/outer diameter ratio decreases with increasing sheath flow rate as more sheath material is pumped to the fibers. Typical morphologies of the microfibers are shown in Figure 3c-f for different sheath flow rates. In all these cases, we have produced high quality fibers. Compared to the core flow rate, it is more convenient to tune the fiber diameters using the sheath flow rate as the effect of sheath flow rate on fiber diameters follows a monotonic rather than strongly nonlinear relation.

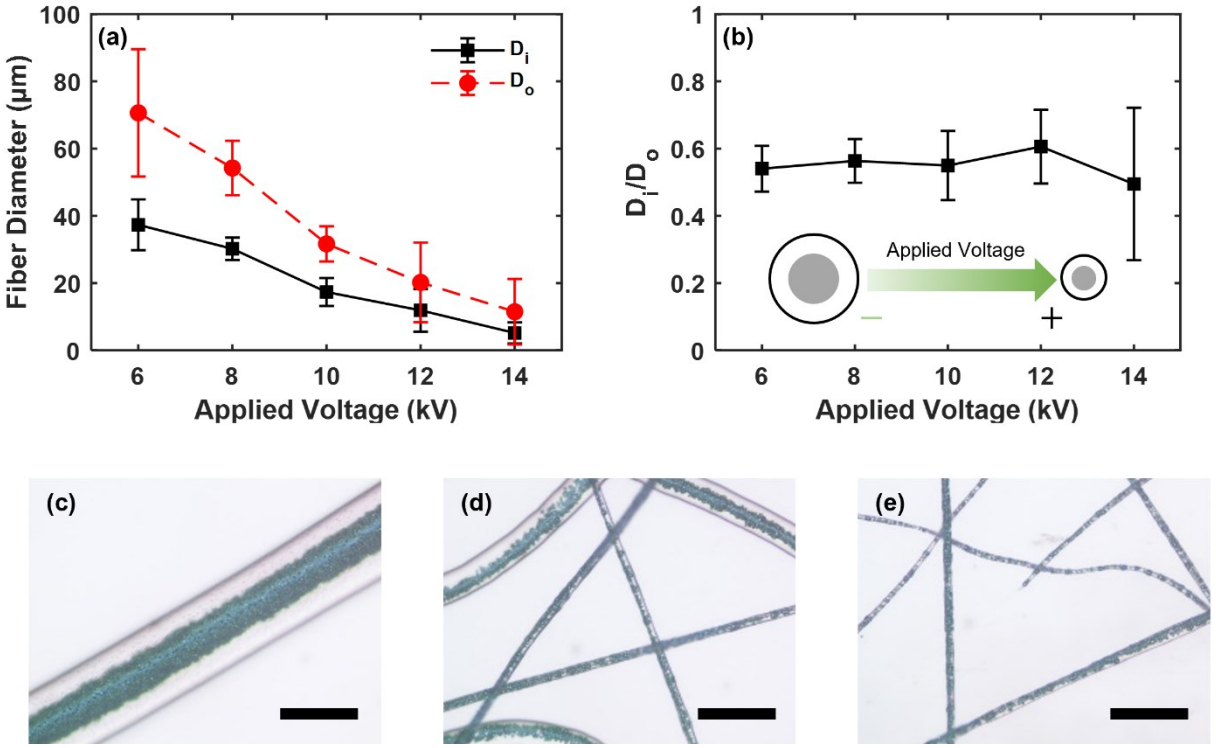

Figure 4. Effect of applied voltage on the electrospinning of coaxial LM microfibers. (a) The inner and outer diameters; (b) The inner/outer diameter ratio D_i/D_o. Some typical OM images of electrospun microfiber samples with different applied voltage: (c) 6 kV; (d) 12 kV; (e) 14 kV, scale bar: 100 μm.

Finally, the effect of voltage is studied. In this case, the core and sheath flow rates are maintained at 0.5 ml/h and 3.5 ml/h, respectively. The applied voltage is adjusted within a range from 6 kV to 14 kV. As shown in **Figure 4**a, both the inner and outer diameters decrease when the voltage increases because of higher electrical force stretching the fibers. So the influence of applied voltage to the fiber diameters is in oppose to the sheath flow rate. This trend is also consistent to the electrospinning of pure polymer solutions.[45,47] If the voltage is below 6 kV, no fibers were produced as the electrical force was too weak. When the voltage is between 6 kV and 12 kV, no bending instability occurs and only a single fiber jet is observed between the needle and the collector during electrospinning (Figure S3b, Supporting Information). For voltage at 12 kV or higher, bending instability occurs and one can collect a fiber mat (Figure S3c, Supporting Information). Figure 4b shows that the inner/outer diameter ratio is almost constant because the core and sheath flow rates are fixed. Figure 4c presents typical morphologies of fibers under different voltage. It is found that for cases with 12 kV and 14 kV, the fibers are over-stretched because of the large electrical stretching force, resulting in discontinuity of the LM core and manufacturing defects. Such defects are detrimental to the electrical conductance of the LM fibers. So one must consider the role of manufacturing defects on the percolation and conductivity of these LM fibers.[49]

In summary, we studied the influences of core flow rate, sheath flow rate, and applied voltage on the fiber diameters and morphologies. Major factors affecting the fiber diameters include the electrical stretching effect, material volume in the core, and material volume in the sheath. The fiber diameters are dictated by the volume effect, stretching effect, and their competition. The volume effect originates from conservation of mass as more material supply tend to thicken the fibers, e.g., by increasing core or sheath flow rate. In contrast, the stretching effect originates from the Coulomb force that stretches the fibers longer and thinner. The stretching effect can be enhanced by either applying higher voltage or increasing solution conductivity (e.g., higher core flow rate). Note that higher core flow rate enhances both the volume effect and stretching effect. These two effects have opposed influence on the fiber diameters, which explains the non-monotonic relation between the core flow rate and fiber diameters. High quality fibers (Figure S5, Supporting Information) can be obtained by optimizing these parameters, especially the sheath flow rate. The electrospinning of LM emulsion is much more complicated than polymers due to the much higher conductivity and dielectric constant of the former.

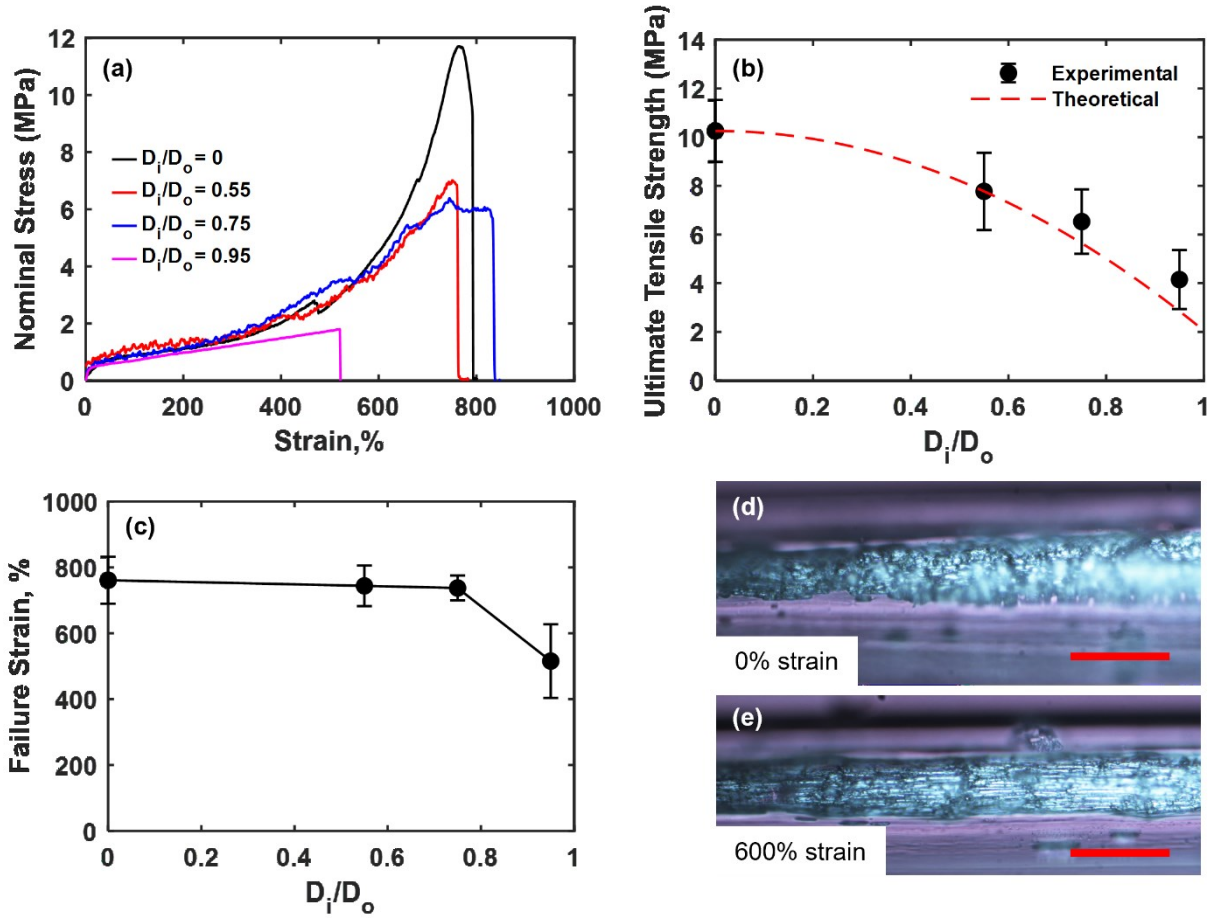

Figure 5. Mechanical testing of coaxial LM microfibers. (a) Comparison of the stress-strain curves of four typical fiber samples with various D_i/D_o ratios. (b) Ultimate tensile strength of LM microfibers with different D_i/D_o. (c) Failure strain of LM microfibers with different D_i/D_o. Optical microscopy image of LM microfiber at (d) 0% strain and (e) 600% strain after stretching, scale bar: 50 μm.

2.2. Electromechanical Properties

The mechanical properties of single fibers are tested first. Core-sheath fibers with different inner/outer diameters are tested and compared, where the case D_i/D_o=0 indicates pure SEBS fibers. The stress-strain relations are illustrated in **Figure 5**a. Most of these fibers exhibit hyperelastic behaviors similar to the thermoplastic elastomer SEBS. They are super stretchable with maximum strain up to 800%, comparable to pure SEBS. Figure 5b and 5c compare the tensile strength and failure strain of these coaxial fibers, respectively. As the inner/outer diameter ratio increases, the tensile strength gradually decreases, revealing that more LM in the coaxial fiber deteriorates the mechanical strength. Provided that the LM phase offers no

mechanical strength, we can estimate the tensile strength of the coaxial fiber using the rule of mixture, as

$$\boldsymbol{\sigma_f = \sigma_f^{SEBS}\left[1 - V_{LM}\left(\frac{D_i}{D_o}\right)^2\right]} \quad (1)$$

where $\boldsymbol{\sigma_f}$ and $\boldsymbol{\sigma_f^{SEBS}}$ are the tensile strength of the coaxial microfiber and SEBS, respectively; $\boldsymbol{V_{LM} = 0.8}$ is the volume ratio of LM in the core. The theoretical prediction in Equation (1) agrees very well to the experimental data in Figure 5b. Figure 5c further explores the failure strain of these coaxial fibers. In most cases, the stretchability of the coaxial fibers is dominated by the SEBS sheath. In the case with ultrathin sheath (D_i/D_o = 0.95), the coaxial fibers break prematurely but still have a mean failure strain around 500%. In summary, the mechanical testing data of single fibers indicate that their tensile strength and stretchability are dominated by the sheath layer. The fluidic nature of the LM phase offers negligible mechanical strength for the coaxial fibers but helps to maintain their high stretchability. As shown in Figure 5d, the LM particles are stretched into needle shapes under 600% strain. This behavior is different from hard conductive fillers such as silver or graphite powders.[50] The electrical properties of the fibers were not tested because they become very fragile after sintering. Instead, we evaluated the electrical properties of the fiber mat.

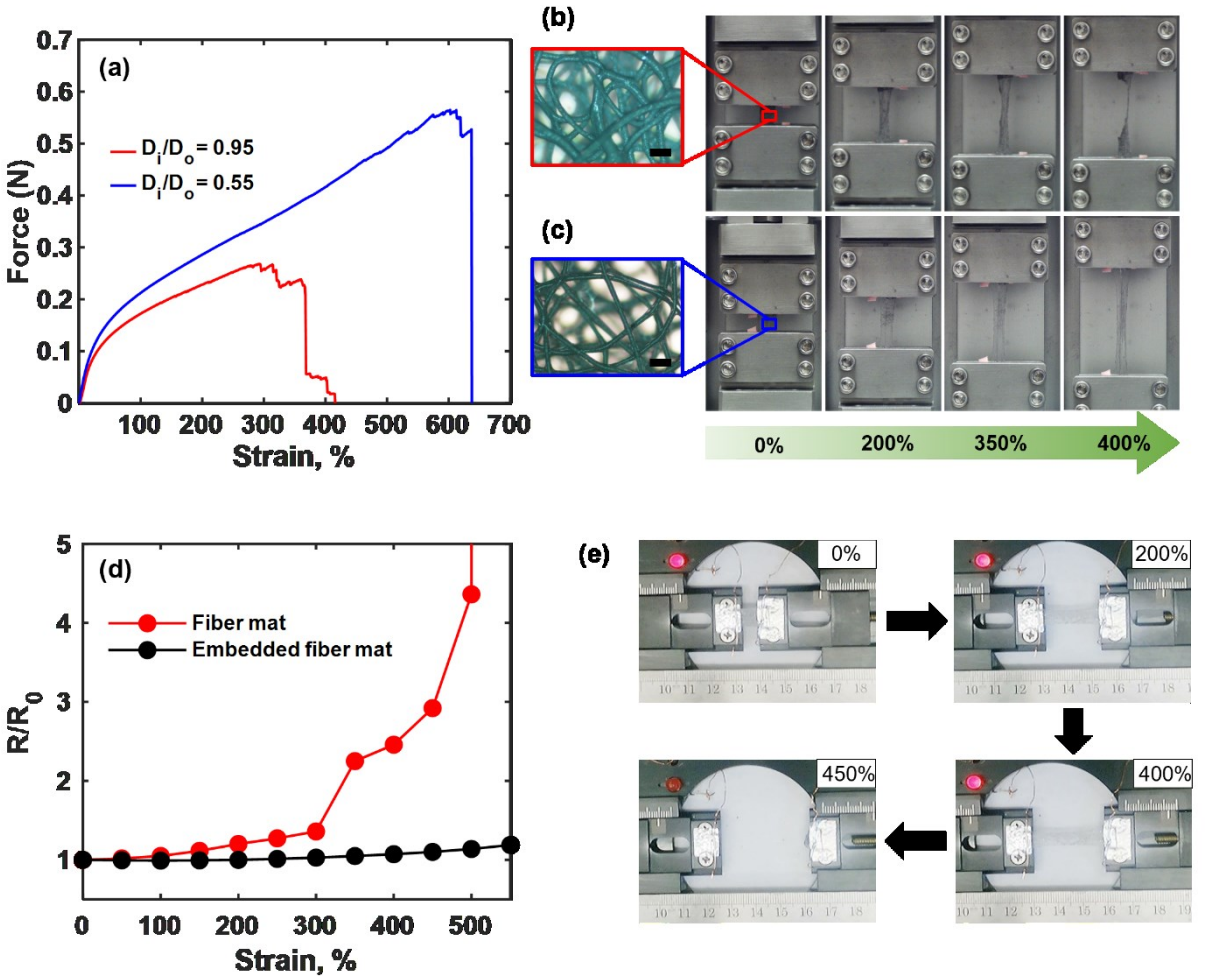

Figure 6. Tensile testing of LM fiber mat: (a) The force-strain curves for fiber mat samples with different D_i/D_o. (b) and (c) show the evolution of LM fiber mats during tensile testing at different applied strain for D_i/D_o as 0.95 and 0.55, respectively, scale bar: 200 µm. (d) The comparison of normalized resistance R/R_0 as a function of strain for the non-embedded (D_i/D_o as 0.95) and embedded fiber mats. (e) Photographs displaying the brightness of LED at various strain levels for a LM fiber mat with D_i/D_o = 0.95.

The electromechanical behavior of the coaxial fiber mat is presented in **Figure 6**. Figure 6a shows the typical force-strain curves of two fiber mats with different inner/outer diameter ratios (Figure S4, Supporting Information). The mat with thick sheath layer (D_i/D_o = 0.55) was stretched up to 630% of strain, whereas the mat with thin sheath layer (D_i/D_o = 0.95) was stretched up to 400% until failure. The mat is overall highly stretchable but fragile if not embedded in an elastomer matrix. By comparing the force-strain curves in Figure 6a and the failure process in Figure 6b, we observe that failure of the mat occurs at the peak force level when a crack initiates and propagates quickly along the transverse direction. Electromechanical

properties of the mat are presented in Figure 6c. The mat is mechanically sintered to be conductive before testing. The normalized resistance R/R_0 of the mat increases suddenly at 300% strain, indicating accumulated damage of the percolation paths. In contrast, once embedded in an elastomer matrix, the normalized resistance is very stable. The electromechanical behaviors of LM fiber mat embedded in a matrix have been reported in previous work and will not be repeated here.[11]

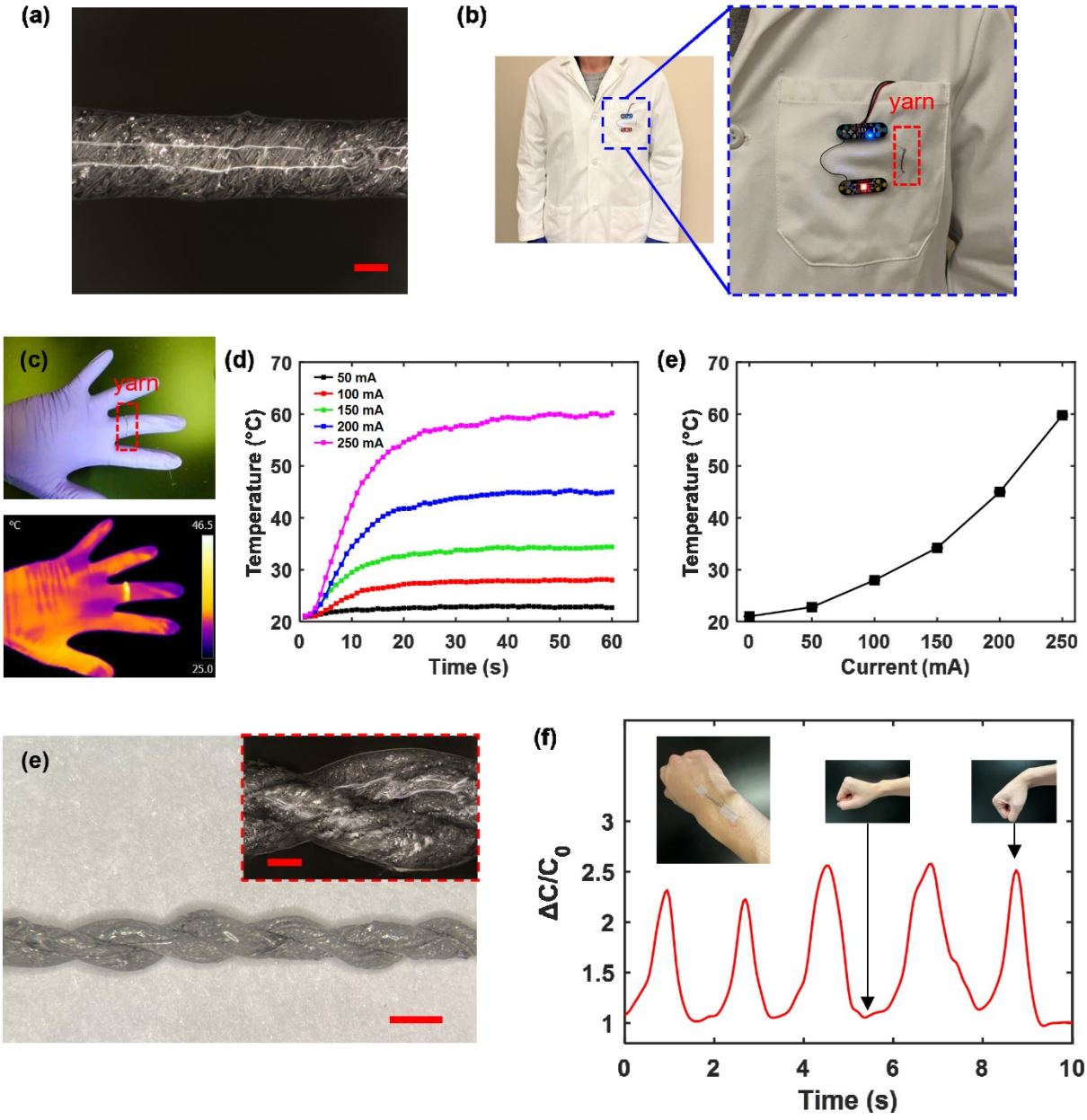

Figure 7. Applications of LM fiber yarns. (a) Optical microscopy image of a LM fiber yarn. Scale bar: 200 µm. (b) Application of the yarn as wearable interconnect for a circuit. (c) Application of the yarn as a joule heater. The temperature profile is presented. (d) Joule

heating performance of a LM yarn. (e) Maximum temperature of the yarn-based heater under various currents. (e) Optical microscopy image of a capacitance strain sensor made of two strands of LM yarns. Scale bar: 1 mm. Inset scale bar: 200 μm. (f) Capacitance response of the capacitance strain sensor under wrist motion.

2.3. Applications as Yarns

From the application perspective, the produced LM fibers or mat after sintering are either too fragile or electrically unstable to be used directly. Our previous work showed that composites embedded with LM fibers are super-stretchable conductors with excellent electromechanical performance.[11] These composites could be used as soft electrodes, interconnects, and sensing purposes. In this work, we will present an alternative application of LM fibers in the form of yarns.[51,52] LM yarns find potential applications in e-textile, wearable electronics, joule heating, and sensing.

Figure 7 presents various applications of LM fiber yarns. The yarn structure offers improved mechanical strength and reliability compared to single fibers. They are electrically conductive if sintered beforehand. A typical yarn structure is shown in Figure 7a. This yarn was used as a stretchable interconnect in Figure 7b and a joule heater in Figure 7c for applications in wearable electronics. The heating performance of the yarn-based joule heater was tested and presented in Figure 7d-e. Under various currents, the heater usually reached their balanced temperature within 10-20 seconds. In addition, the yarn can also be used as capacitance sensor if two strands of LM yarns are twisted together, as shown in Figure 7e. Note that a dielectric layer is needed between the two strands. In this case, the LM fibers serve as the electrode and the silicone encapsulate and SEBS sheath serve as the dielectric material. Under stretching or pressing, the capacitance of the LM yarns would change, serving as the sensing mechanism.[23] An example is shown in Figure 7e, where such a capacitance sensor is attached to a wrist, which monitors the motion of the wrist. In brief summary, the LM fiber yarns can be readily used in electronics as soft conductors.

3. Conclusions

In this work, we performed a systematic study on the electrospinning process of coaxial LM fibers for multifunctional applications. These microfibers are super-stretchable due to the SEBS sheath and highly conductive because of the LM core. High quality of coaxial LM microfibers have been fabricated with fiber diameters of 10-100 microns, which are much

thinner than the liquid metal fibers reported in the literature (mostly 100-1000 microns). We have studied influences of various electrospinning processing parameters on the diameters and morphologies of the coaxial fibers. It was discovered that the core flow rate, sheath flow rate, and applied voltage are dominant factors affecting the fiber diameters and morphologies. The inner/outer diameter ratio of the coaxial fiber is mainly affected by the core and sheath flow rates but not the applied voltage. Due to the high conductivity and dielectric constant of the LM emulsion, the electrospinning process exhibits distinct features compared to pure polymers. Experiments and theoretical analysis show that the liquid metal microfibers normally have impaired tensile strength when the liquid metal content increases. In contrast, the stretchability of the liquid metal fibers is usually close to that of SEBS unless the sheath is extremely thin. The developed coaxial LM fibers can be made into the forms of composites or yarns and applied as soft conductors in flexible and wearable electronics, joule heaters, sensors, energy harvesting, etc.

Future works can be towards further improving the electrical conductivity of the coaxial fibers. This may be achieved through increasing the liquid metal content in the core emulsion, provided that sedimentation of particles does not occur. In addition, the current fiber still needs mechanical sintering to activate the conductivity. However, the sintering process is usually challenging to control as incomplete or nonuniform sintering may exist. This is a critical challenge that deserves further investigation in the future. In addition, scale up manufacturing is also one great opportunity to reduce cost and further develop this technology for electronics applications. Scale up manufacturing of LM fibers needs to tackle multiple challenges such as mass production of LM particles, mixing of emulsions, and special spinet designs for multi-jet production of fibers.

4. Experimental Section

Materials: The SEBS polymer used in this work is Kraton G1657. It is a clear, linear triblock copolymer based on styrene and ethylene/butylene with a polystyrene content of 13%. Gallium (99.99%) and indium (99.995%) bigots were acquired from Luciteria Science. Chloroform and toluene were purchased from Macron Fine Chemical and Honeywell, respectively. 1-Dodecanethiol (≥98%) was purchased from Sigma Aldrich. All chemicals used as received without further purification.

LM Synthesis: To synthesize the LM eutectic Gallium-Indium (EGaIn, Ga75.5In24.5), gallium and indium pellets were put in a glass vial and heated at 175°C for 3 hours in a vacuum

furnace. Then, the molten alloy was mixed by a magnetic stirrer at 100 rpm for 30 min on a hot plate at 90°C. After mixing, the alloy was heated again at 175°C for 2 hours in a vacuum furnace to ensure the alloying is complete.

Solution Preparation: For the SEBS sheath solution, SEBS pellets were dissolved in a binary solvent chloroform/toluene (80/20 by weight). The weight percentage of SEBS in the sheath solution is 16 wt% for coaxial emulsion electrospinning and 10-20 wt% for SEBS fiber electrospinning. The sheath solution was homogenized by a vortex mixer for 24 h for electrospinning usage. For the LM core emulsion, EGaIn was added into a mixture of chloroform and 1-Dodecanethiol (1 mM/g) in a glass vial first. Note that 1-Dodecanethiol was added to make the oxide shell easier to rupture.[53] EGaIn microparticles were produced using an ultrasonic probe (Branson 450 Sonifier) with 40% amplitude for 30 min (Figure S2, Supporting Information). The obtained EGaIn microparticles were mixed with SEBS, chloroform, and toluene to obtain a viscous LM emulsion (EGaIn:SEBS = 4:1 by volume). The ratio of SEBS, chloroform, and toluene was 9:72.8:18.2 by weight. The emulsion was further homogenized by a vortex mixer for 24 h followed by bath sonication (Branson 1510) for 1 h. Both the sheath solution and core emulsion were prepared right before electrospinning.

Electrospinning Process: The core emulsion and sheath solution were transferred to 3 mL syringes, respectively. As shown in Figure 1, the coaxial electrospinning system consists of two single channel syringe pumps (NE-300, New Era Pump System Inc.), a 17/22-gauge coaxial needle (VECK, China), a DC high-voltage power supply (P030HP1, Acopian, USA), and a flat aluminum plate used as a collector. The electrospinning setup was installed in a fume hood. Major processing parameters include core flow rate, sheath flow rate, voltage, and tip-to-collector distance. In order to study the influence of processing parameters, the tip-to-collector distance was fixed at 16 cm while other parameters were changed. After electrospinning, the electrospun fibers and mats were air-dried for 12 hours in a fume hood.

Electromechanical Measurements: Electrospun microfibers and mats were cut into suitable sizes for testing. For mechanical testing, a tensile tester with 5 N load cell was used (ADMET eXpert4000). For electrical testing, the resistance of electrospun fiber mat was measured by a Keithley 6514 electrometer. Before the electrical resistance testing, all of the microfiber mat samples were mechanically sintered manually by applying pressure using a smooth steel rod. In addition, aluminum conductive tapes were used to make good connection between samples and alligator clips of the electrometer.

Testing of Fiber Yarn: For the LM fiber yarns, they were fabricated by twisting a pre-sintered fiber mat and then encapsulated in silicone (ExoFlex 00-30, Smooth-on Inc.). The fiber yarns were used as interconnects and joule heaters. In the heating experiment, the temperature profile was measured using an infrared camera. For the application as capacitance sensors, two encapsulated fiber yarns were twisted together as two strands and then encapsulated in silicone. The capacitance was measured by a Keithley 2110 multimeter.

Though deemed not to be human subjects research by the Binghamton University Institutional Review Board, IRB guidelines for providing informed consent were followed.

Supporting Information

Supporting Information is available from the Wiley Online Library or from the author.

Acknowledgements

This work is supported by the National Science Foundation through the award CMMI-2143297. The authors also thank the support from the Small Scale Systems Integration and Packaging (S3IP) Center of Excellence, funded by the New York Empire State Development's Division of Science, Technology, and Innovation.

Received: ((will be filled in by the editorial staff))
Revised: ((will be filled in by the editorial staff))
Published online: ((will be filled in by the editorial staff))

Reference

[1] W. Babatain, M. S. Kim, M. M. Hussain, *Adv Funct Materials* **2024**, *34*, 2308116.
[2] Z. Zhao, S. Soni, T. Lee, C. A. Nijhuis, D. Xiang, *Advanced Materials* **2023**, *35*, 2203391.
[3] M. D. Dickey, *Advanced Materials* **2017**, *29*, 1606425.
[4] S. Chen, H.-Z. Wang, R.-Q. Zhao, W. Rao, J. Liu, *Matter* **2020**, *2*, 1446.
[5] N. Kazem, T. Hellebrekers, C. Majidi, *Advanced Materials* **2017**, *29*, 1605985.
[6] P. Won, S. Jeong, C. Majidi, S. H. Ko, *iScience* **2021**, *24*, 102698.
[7] M. Reis Carneiro, C. Majidi, M. Tavakoli, *Adv Funct Materials* **2023**, *33*, 2306453.
[8] A. Fassler, C. Majidi, *Advanced Materials* **2015**, *27*, 1928.

[9] R. Tutika, S. Kmiec, A. B. M. T. Haque, S. W. Martin, M. D. Bartlett, *ACS Appl. Mater. Interfaces* **2019**, *11*, 17873.

[10] A. B. M. T. Haque, R. Tutika, R. L. Byrum, M. D. Bartlett, *Adv Funct Materials* **2020**, *30*, 2000832.

[11] J. Ma, Z. Liu, Q. Nguyen, P. Zhang, *Adv Funct Materials* **2024**, *34*, 2308128.

[12] F. Deng, Q.-K. Nguyen, P. Zhang, *Additive Manufacturing* **2020**, *33*, 101117.

[13] F. Deng, Q.-K. Nguyen, P. Zhang, *Applied Materials Today* **2022**, *29*, 101671.

[14] B. Yao, W. Hong, T. Chen, Z. Han, X. Xu, R. Hu, J. Hao, C. Li, H. Li, S. E. Perini, M. T. Lanagan, S. Zhang, Q. Wang, H. Wang, *Advanced Materials* **2020**, *32*, 1907499.

[15] P. Yang, X. Li, X. Yang, G. Li, Z. Hu, L. Huang, Y. Wu, *Adv Funct Materials* **2022**, *32*, 2205167.

[16] H. Choi, Y. Luo, G. Olson, P. Won, J. H. Shin, J. Ok, Y. J. Yang, T. Kim, C. Majidi, *Adv Funct Materials* **2023**, *33*, 2301388.

[17] L. Zheng, M. Zhu, B. Wu, Z. Li, S. Sun, P. Wu, *Sci. Adv.* **2021**, *7*, eabg4041.

[18] S. Zhu, J. So, R. Mays, S. Desai, W. R. Barnes, B. Pourdeyhimi, M. D. Dickey, *Adv Funct Materials* **2013**, *23*, 2308.

[19] H. Wang, R. Li, Y. Cao, S. Chen, B. Yuan, X. Zhu, J. Cheng, M. Duan, J. Liu, *Adv. Fiber Mater.* **2022**, *4*, 987.

[20] Z. Ma, Q. Huang, Q. Xu, Q. Zhuang, X. Zhao, Y. Yang, H. Qiu, Z. Yang, C. Wang, Y. Chai, Z. Zheng, *Nat. Mater.* **2021**, *20*, 859.

[21] Q. Zhuang, Z. Ma, Y. Gao, Y. Zhang, S. Wang, X. Lu, H. Hu, C. Cheung, Q. Huang, Z. Zheng, *Adv Funct Materials* **2021**, *31*, 2105587.

[22] M. Zheng, A. Li, X. He, L. Wang, X. Qin, *Nano Energy* **2024**, *129*, 110078.

[23] C. B. Cooper, K. Arutselvan, Y. Liu, D. Armstrong, Y. Lin, M. R. Khan, J. Genzer, M. D. Dickey, *Advanced Functional Materials* **2017**, *27*, 1605630.

[24] C. Dong, A. Leber, T. Das Gupta, R. Chandran, M. Volpi, Y. Qu, T. Nguyen-Dang, N. Bartolomei, W. Yan, F. Sorin, *Nat Commun* **2020**, *11*, 3537.

[25] S. Mun, S. Lee, K. J. Bae, Y. Bae, H.-M. Lee, B.-J. Kim, J. Yu, S. Park, *Adv. Fiber Mater.* **2024**, *6*, 900.

[26] P. Bhuyan, M. Singh, Y. Wei, D. Thanh Tran, M. Ha, K.-U. Jeong, H. Jeon, S. Park, *Chemical Engineering Journal* **2024**, *480*, 147944.

[27] M. A. H. Khondoker, A. Ostashek, D. Sameoto, *Adv Eng Mater* **2019**, *21*, 1900060.

[28] Z. Lin, X. Qiu, Z. Cai, J. Li, Y. Zhao, X. Lin, J. Zhang, X. Hu, H. Bai, *Nat Commun* **2024**, *15*, 4806.

[29] L. Zhou, J. Fu, Q. Gao, P. Zhao, Y. He, *Adv Funct Materials* **2020**, *30*, 1906683.

[30] M. Song, K. Kartawira, K. D. Hillaire, C. Li, C. B. Eaker, A. Kiani, K. E. Daniels, M. D. Dickey, *Proc. Natl. Acad. Sci. U.S.A.* **2020**, *117*, 19026.

[31] L. Long, X. Che, P. Yao, X. Zhang, J. Wang, M. Li, C. Li, *ACS Appl. Mater. Interfaces* **2022**, *14*, 18690.

[32] Y. Yu, J. Guo, B. Ma, D. Zhang, Y. Zhao, *Science Bulletin* **2020**, *65*, 1752.

[33] X. Yu, W. Fan, Y. Liu, K. Dong, S. Wang, W. Chen, Y. Zhang, L. Lu, H. Liu, Y. Zhang, *Adv Materials Technologies* **2022**, *7*, 2101618.

[34] Q. Zhang, D. J. Roach, L. Geng, H. Chen, H. J. Qi, D. Fang, *Smart Mater. Struct.* **2018**, *27*, 035019.

[35] H. Li, R. Qu, Z. Ma, N. Zhou, Q. Huang, Z. Zheng, *Adv Funct Materials* **2024**, *34*, 2308120.

[36] N. Zhou, B. Jiang, X. He, Y. Li, Z. Ma, H. Zhang, M. Zhang, *ACS Appl. Mater. Interfaces* **2021**, *13*, 19254.

[37] Y.-G. Park, H. S. An, J.-Y. Kim, J.-U. Park, *Sci. Adv.* **2019**, *5*, eaaw2844.

[38] Y.-G. Park, H. Min, H. Kim, A. Zhexembekova, C. Y. Lee, J.-U. Park, *Nano Lett.* **2019**, *19*, 4866.

[39] S. Ramakrishna, K. Fujihara, W.-E. Teo, T.-C. Lim, Z. Ma, *An Introduction to Electrospinning and Nanofibers*, WORLD SCIENTIFIC, **2005**.

[40] Electrospinning: Nanofabrication and Applications, Elsevier, **2019**.

[41] L. Chen, S. Wang, Q. Yu, P. D. Topham, C. Chen, L. Wang, *Soft Matter* **2019**, *15*, 2490.

[42] L. Wang, P. D. Topham, O. O. Mykhaylyk, H. Yu, A. J. Ryan, J. P. A. Fairclough, W. Bras, *Macromol. Rapid Commun.* **2015**, *36*, 1437.

[43] S. Ribeiro, P. Costa, C. Ribeiro, V. Sencadas, G. Botelho, S. Lanceros-Méndez, *Composites Part B: Engineering* **2014**, *67*, 30.

[44] T. R. Lear, S.-H. Hyun, J. W. Boley, E. L. White, D. H. Thompson, R. K. Kramer, *Extreme Mechanics Letters* **2017**, *13*, 126.

[45] A. Haider, S. Haider, I.-K. Kang, *Arabian Journal of Chemistry* **2018**, *11*, 1165.

[46] V. Beachley, X. Wen, *Materials Science and Engineering: C* **2009**, *29*, 663.

[47] Z. Li, C. Wang, In *One-Dimensional nanostructures*, Springer Berlin Heidelberg, Berlin, Heidelberg, **2013**, pp. 15–28.

[48] B. Sun, Y. Z. Long, H. D. Zhang, M. M. Li, J. L. Duvail, X. Y. Jiang, H. L. Yin, *Progress in Polymer Science* **2014**, *39*, 862.

[49] M. Madadi, P. Zhang, *Soft Matter* **2024**, *20*, 1061.

[50] G. Yun, S.-Y. Tang, H. Lu, S. Zhang, M. D. Dickey, W. Li, *Small Science* **2021**, *1*, 2000080.

[51] Q. Gao, S. Agarwal, A. Greiner, T. Zhang, *Progress in Materials Science* **2023**, *137*, 101139.

[52] D. Kim, Z. Yang, J. Cho, D. Park, D. H. Kim, J. Lee, S. Ryu, S. Kim, M. Kim, *EcoMat* **2023**, *5*, e12384.

[53] L. Mou, J. Qi, L. Tang, R. Dong, Y. Xia, Y. Gao, X. Jiang, *Small* **2020**, *16*, 2005336.

Table of Contents

This work conducts a systematic study on the emulsion electrospinning process of liquid metal fibers with diameters in the range of 10-100 microns. Key processing parameters such as core and sheath flow rates and applied voltage are explored. The fibers and yarns demonstrate super-stretchability and high conductivity, showing promise for use in soft and wearable electronics.

Z. Liu, J. Ma, P. Zhang*

Fabrication of Stretchable and Conductive Liquid Metal Microfibers Through Coaxial Emulsion Electrospinning

ToC figure (size: 55 mm broad × 50 mm high)

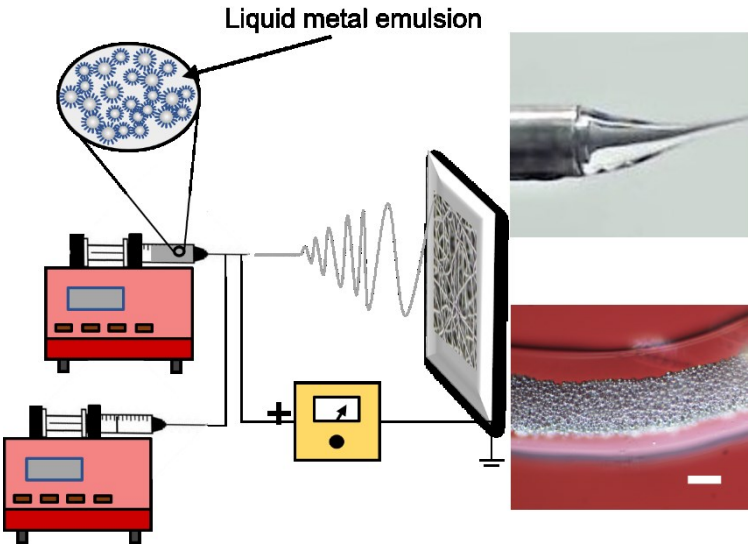

Supporting Information

Fabrication of Stretchable and Conductive Liquid Metal Microfibers Through Coaxial Emulsion Electrospinning

*Zihan Liu, Jiexian Ma, and Pu Zhang**

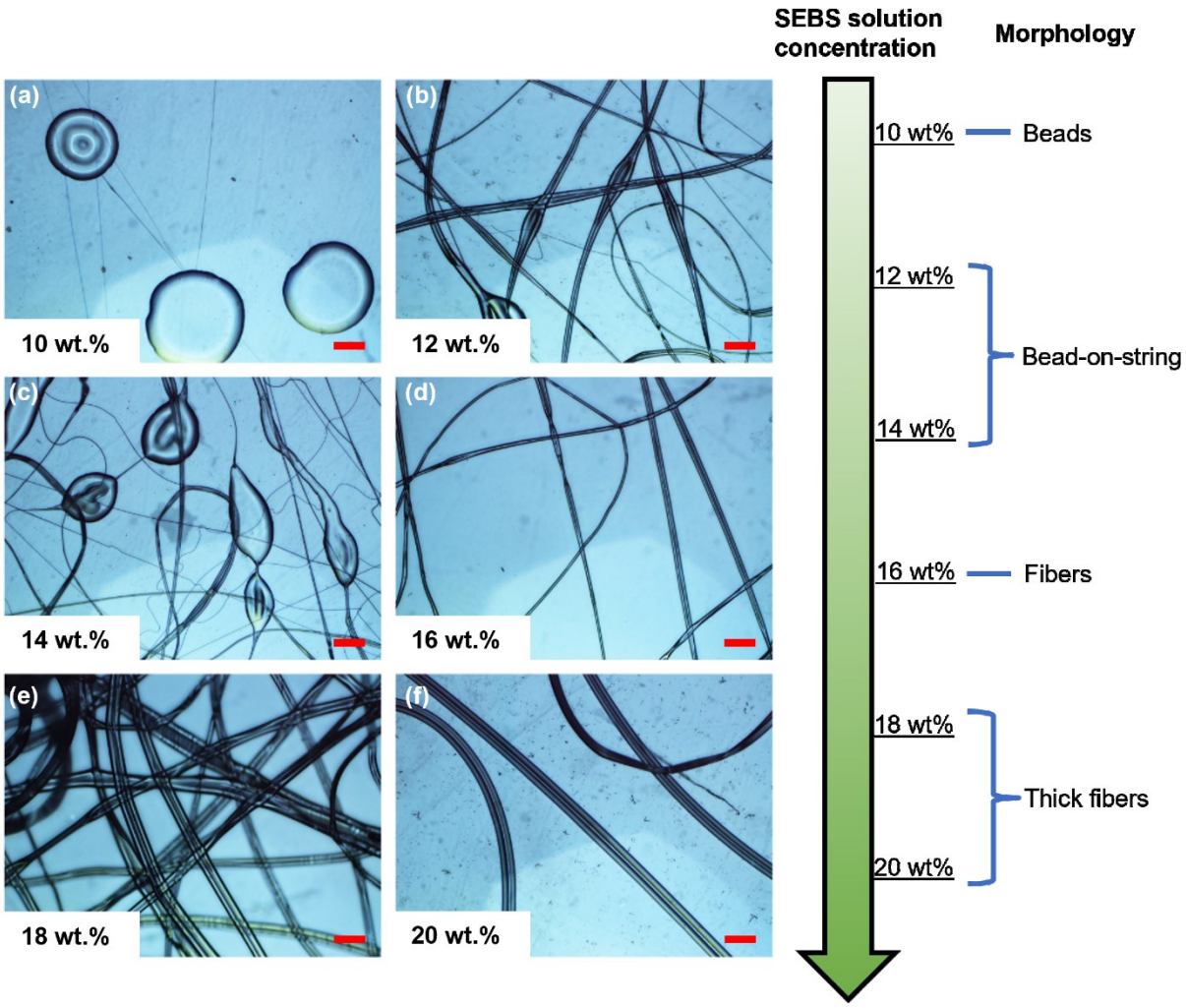

Figure S1. Electrospinning of pure SEBS fibers using solutions with various concentrations of SEBS in the binary solvent (gauge-22 needle). (a) 10 wt%; (b) 12 wt%; (c) 14 wt%; (d) 16 wt%; (e) 18 wt%; (f) 20 wt%. The morphologies change from beads to fibers as expected. Scale bar: 200 μm.

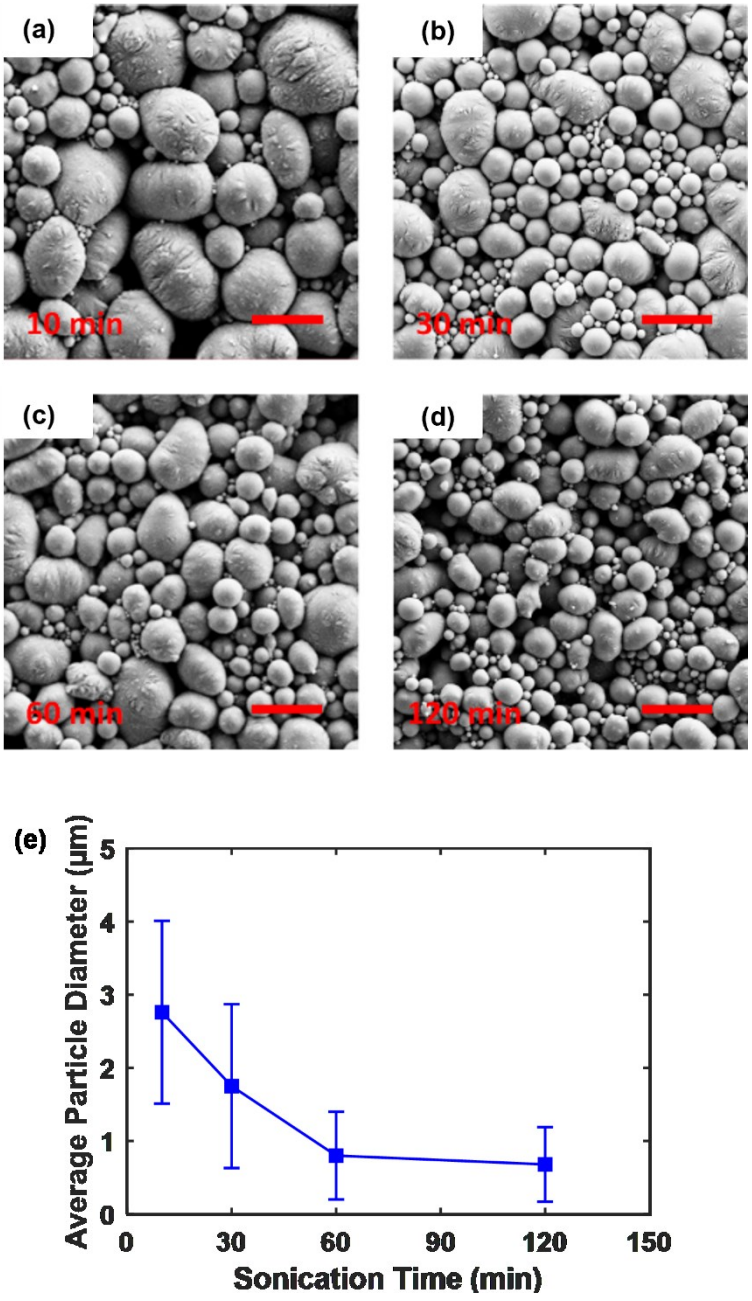

Figure S2. SEM images of liquid metal particles produced at different sonication time: (a) 10 min; (b) 30 min; (c) 60 min; (d) 120 min. The amplitude of the sonication probe is set at 40% for all cases. (e) The average particle diameter versus sonication time. Scale bar: 4 μm. For each sonication time, we measured at least 50 particles to determine the particle size range.

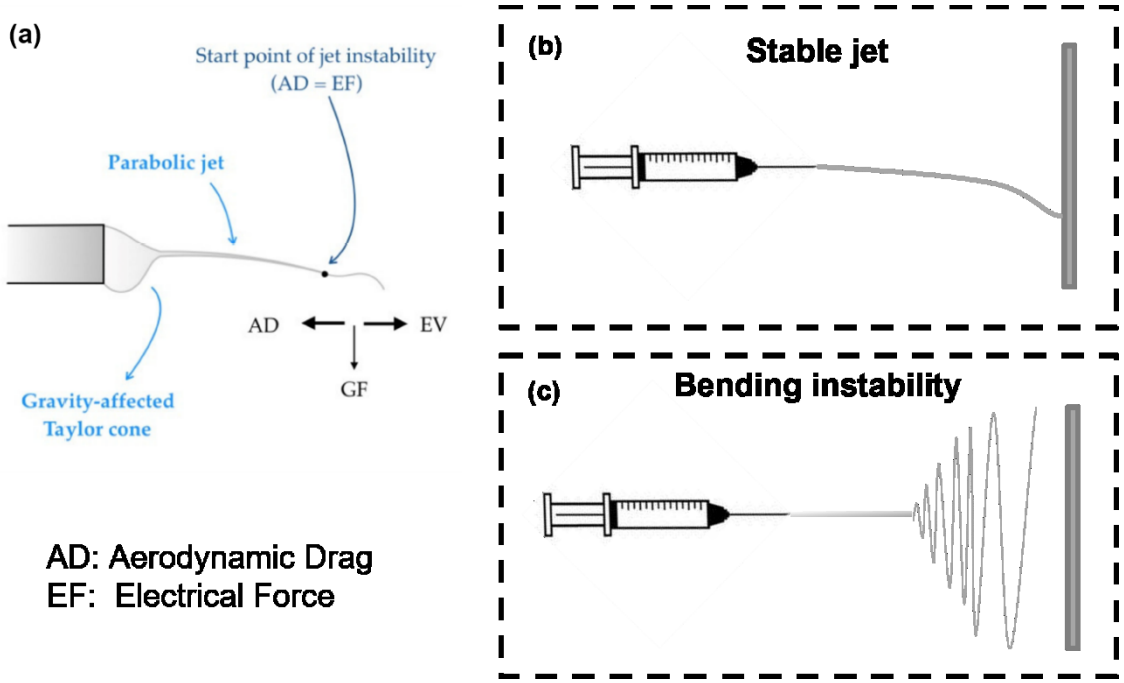

Figure S3. Influence of voltage on the jetting instability of electrospinning. (a) Balance of various forces. Reproduced with permission[1]. (b) At low voltage, a stale jet is formed. (c) At high voltage, bending instability occurs.

[1] S. Suresh, A. Becker, B. Glasmacher, *Polymers* **2020**, *12*, 2448.

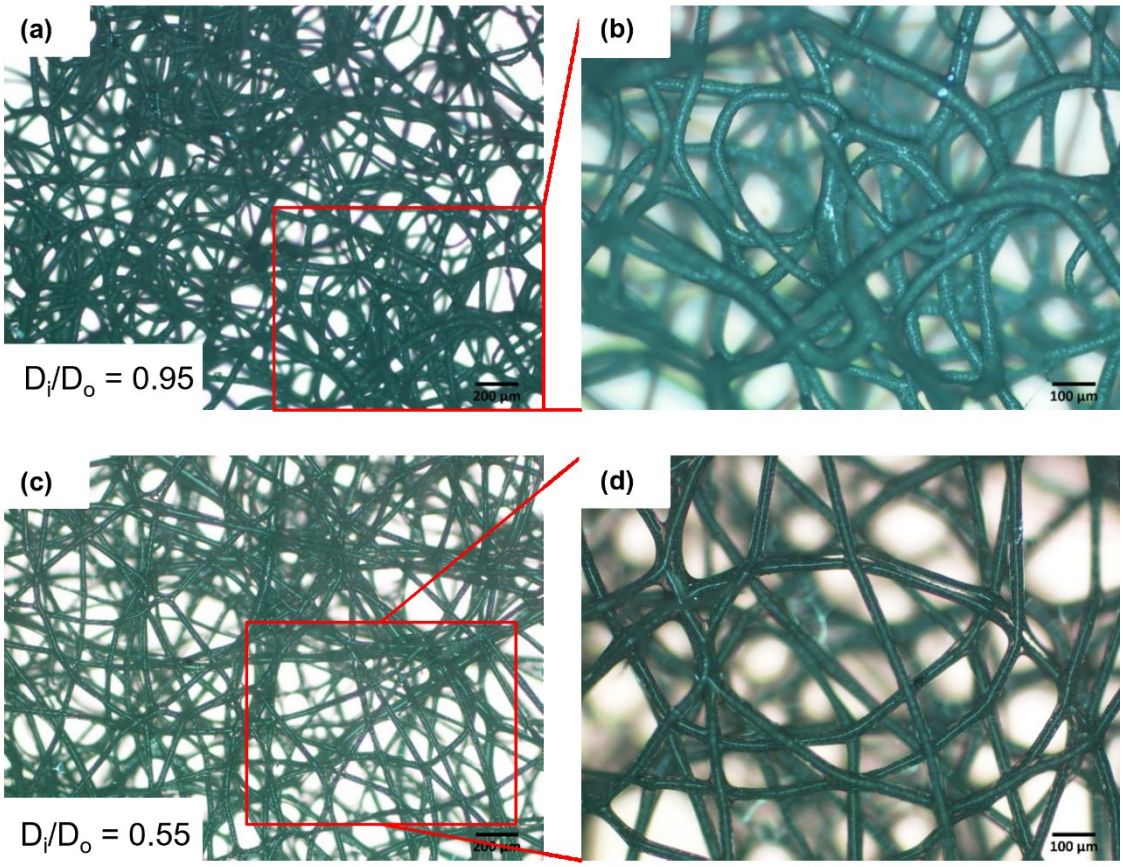

Figure S4. Optical microscopy images of LM microfiber mat with different inner/outer diameter ratios. (a-b) D_i/D_o = 0.95 and (c-d) D_i/D_o = 0.55.

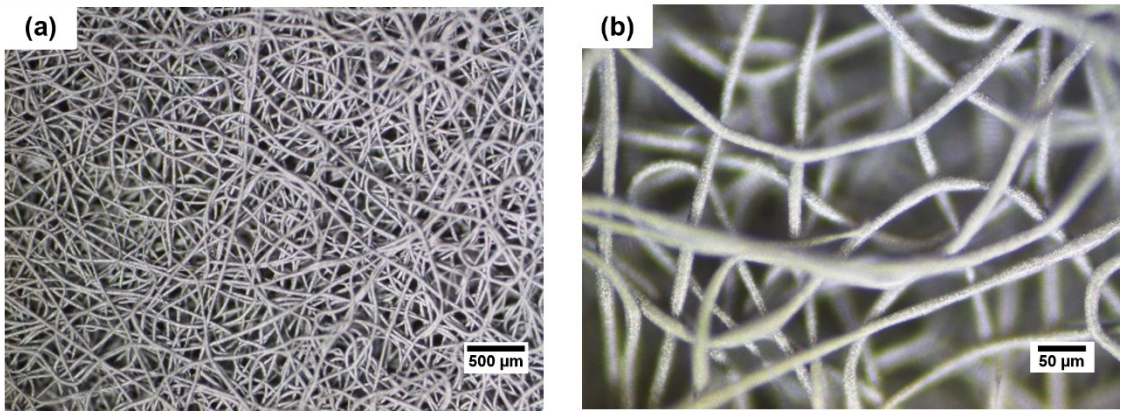

Figure S5. SEM images of typical LM microfiber mats produced through coaxial emulsion electrospinning. Uniform and smooth fibers were observed.